ACS APPLIED MATERIALS & INTERFACES

Research Article

www.acsami.org

Cooperative Effect of pH-Dependent Ion Transport within Two Symmetric-Structured Nanochannels

Zheyi Meng, Yang Chen, Xiulin Li, Yanglei Xu, and Jin Zhai*

Key Laboratory of Bio-Inspired Smart Interfacial Science and Technology of Ministry of Education, School of Chemistry and Environment, Beihang University, Beijing 100191, P. R. China

Supporting Information

ABSTRACT: A novel and simple design is introduced to construct bichannel nanofluid diodes by combining two poly(ethylene terephthalate) (PET) films with columnar nanochannel arrays varying in size or in surface charge. This type of bichannel device performs obvious ion current rectification, and the pH-dependent tunability and degree of rectification can be improved by histidine modification. The origin of the ion current rectification and its pH-dependent tunability are attributed to the cooperative effect of the two columnar half-channels and the applied bias on the mobile ions. As a result of surface groups on the bichannel being charged with different polarities or degrees at different pH values, the function of the bichannel device can be converted from a nanofluid diode to a normal nanochannel or to a reverse diode.

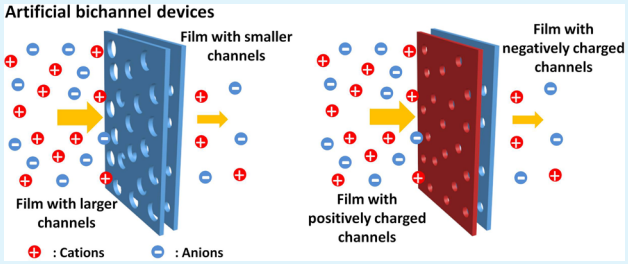

KEYWORDS: *ion transport, biomimetics, nanofluid diode, bichannel device, PET film, columnar nanochannel*

INTRODUCTION

In nature, biological ion channels in cell membranes play vital roles in materials and information exchange between a cell and its surroundings or other cells.[1,2] Direct cell-to-cell communications, which exist in coordinated activities between cells in higher animals, such as embryogenesis, also rely on a family of specified ion channels, which are not single-channel proteins but multiple ones, namely, gap junction channels.[3−5] An entire gap junction channel bridging the membranes of two adjacent cells is constructed from the association of two half-channels supplied separately by each of the two participating cells. Based on the cooperative effect of the two half-channels in molecular size, gap junction channels allow intercellular transmissions of ions or smaller informational molecules but prevent the movements of larger proteins or nucleic acids. The structure of gap junction channels inspired us to propose a new design for constructing artificial ion channels by associating double synthetic nanochannels with varying size or surface charge together and applying their cooperative effect on ions to achieve ionic selectivity.

The asymmetric ion transport of artificial ion channels is often characterized in rectified ion currents, which are similar to those of semiconductor diodes. Therefore, artificial ion channels are also called nanofluidic diodes. Nanofluidic diodes have been well developed in the past few decades,[6,7] such as alumina,[8−10] silica,[11−13] and titania[14,15] nanochannel arrays; ion- and electron-beam-etched silicon and silicon nitride films;[16−18] quartz nanopipettes;[19−23] and track-etching polymer films,[24−27] generally inspired by single-ion channels. Studies of multiple nanofluidic diodes mimicking the structure of gap junction channels started just a few years ago.[28−31] The most common are alumina-based double-/triple-nanofluid devices,[32−35] which result from the association of macroporous alumina arrays with mesoporous materials, such as carbon or silica. They perform well for molecule separation or nanogating for ions, but they are not easy to synthesize. In recent years, with the development of track-etching polymer films, polymer-based double nanofluid devices[30,36,37] (so-called bichannel devices) have been designed by combining two polymer nanochannels or mesoporous silica and polymer nanochannels, because of their low-cost and simple preparation. However, the ion-transport properties of polymer-based bichannel devices corresponding to external stimuli were not discussed in these earlier studies.

Here, we introduce a novel and simple design for constructing bichannel nanofluid diodes by combining two poly(ethylene terephthalate) (PET) films with columnar nanochannel arrays varying in size or in surface charge and study the cooperative effect of pH-dependent ion transport in the device (Scheme 1). Because of the regular shape of the nanochannel and its negatively charged and modifiable surface, track-etched PET nanoporous films have been applied in the fabrication of various nanofluidic diodes in the field of sensors.[38−41] Unlike Zeng et al.'s bichannel devices consisting of two single conical PET nanochannels,[37] here, we introduce PET films with columnar nanochannel arrays into the bichannel device. The symmetric structure of the PET nanochannels removes the effect of asymmetry in geometry or composition

Received: January 21, 2015
Accepted: March 25, 2015
Published: March 25, 2015

DOI: 10.1021/acsami.5b00647
ACS Appl. Mater. Interfaces 2015, 7, 7709−7716

Scheme 1. Contrast of Natural Bichannel Systems and Artificial Bichannel Devices, where Artificial Bichannel Devices Composed of Two Poly(ethylene terephthalate) (PET) Films with Columnar Nanochannel Arrays Varying in Size or in Surface Charge Achieve Their Asymmetric Ion Transport from the Cooperative Effect of Their Half-Channels

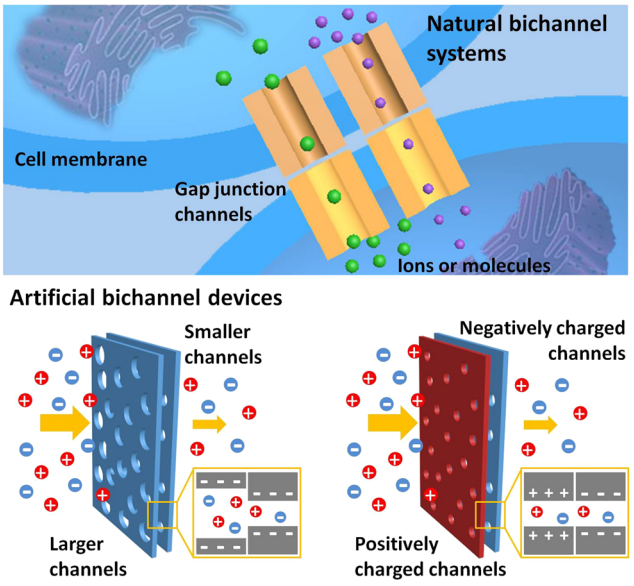

on the ion transport in each half-channel of the bichannel device; in such a situation, the ion current rectification of the bichannel can be attributed completely to the cooperation of the two participating nanochannels, which simplifies the analysis of the origin of ionic selectivity. In addition, PET films with columnar nanochannel arrays are easy to prepare and modify,[42,43] and varying ion-transport properties of bichannels can be achieved by different arrangements of these PET nanochannels. Furthermore, channel arrays on PET films exert ion transport equivalently to single channels but conduct larger ion currents, so bichannel devices consisting of channel arrays are more immune to the effects of current fluctuations on measurements than their counterparts composed of single channels.[44,45]

EXPERIMENTAL SECTION

Nanochannel Fabrication. PET films irradiated by rapid heavy ions (It4ip, Seneffe, Belgium; thickness, 23 μm; ion track density, 4×10^9 cm^{-2}) were used to fabricate columnar nanochannel arrays by chemical etching. Before etching was performed, each side of the sample was exposed to UV light for 2 h. To produce columnar nanochannel arrays, symmetric etching was performed by completely immersing the PET film in the etching solution (2 M NaOH) at 75 °C. The size of the channels and the number of open channels on each film could be controlled by varying the etching time. Then, the etching was stopped by soaking the film in stopping solution (1 M KCl + 1 M HCOOH) at room temperature, and finally, the film was washed in Milli-Q water (18.2 MΩ) to remove residual salts.

Current−Voltage Measurement. The ion-transport properties of bichannel nanofluid diodes were studied by measuring $I-V$ curves using a Keithley 6487 picoammeter (Keithley Instruments, Cleveland, OH). The bichannel device was formed by stacking two PET films with columnar nanochannel arrays together. The two films wetted by Milli-Q water were carefully placed with their flat sides on top of each other to prevent air bubbles from being trapped between the two films, and they were then mounted between the two chambers of a conductivity cell, which were filled with 0.1 M KCl aqueous solutions of varying pH values. The applied bias in this work was a scanning voltage that varied from −1 to +1 V, and two Ag/AgCl electrodes were used to apply the bias. Each measurement was repeated at least five times to obtain the average current at different voltages.

Histidine Modification. The pH-dependent ionic rectification of the bichannel device can be improved by histidine modification. First, the PET film was immersed in 4 mL of an aqueous solution containing 80 mg of *N*-(3-dimethylaminopropyl)-*N*-ethylcarbodiimide hydrochloride (EDC) and 20 mg of *N*-hydroxysuccinimide sodium (NHSS) for 1 h, to convert the carboxyl groups on the PET film to PET-NHSS esters. After being washed with Milli-Q water, the film was soaked in 0.1 M histidine aqueous solution for 24 h, and histidine was immobilized on the inner wall of the columnar PET nanochannel. Finally, the film was washed with Milli-Q water to remove unreacted histidine. The chemical covalent modification in this system is irreversible.

RESULTS AND DISCUSSION

Columnar porous PET films were prepared by symmetrical chemical etching (details in Experimental Section). The size of the channels and the number of open channels on each film are dependent on the etching time, and both of these factors are reflected in the magnitude of the ion current density in a certain electrolyte solution under a certain bias. Table 1 reports the ion current densities and rectification ratios of four films obtained after different etching times, which were measured under 1 V in 0.1 M KCl buffer at pH 7. Ion current measurements and rectification ratio calculations can also be found in the Experimental Section, and 1 V in 0.1 M KCl buffer represents relatively optimized conditions for the measurement of ion transport within PET nanochannels, according to previous research.[46−48] As the etching time was increased from 1.5 to 3 min, the magnitude of the ion current density through the film correspondingly rose from microamperes to milliamperes. When the etching time was more than 3 min, the ion current was above the measurement range (meaning beyond the milliampere range).

Table 1. Ion Current Densities and Rectification Ratios under 1 V in 0.1 M KCl Buffer at pH 7 of Four Films after Different Etching Times

etching time (min)	ion current density (μA/cm^2)	rectification ratio
1.5	0.166	0.91
2	54.8	1.01
3	1.18×10^3	1.04
>3	above the measurement range	–

We chose the films etched for 2 and 3 min, with pore diameters of 80−90 and 190−200 nm, respectively, for further study (Figure 1). Films with etching times shorter than 2 min were not applied, because a short etching time means that only sporadic channels are provided for ion transport on the film, resulting in a tiny ion current density, which cannot properly reflect the high ionic conductance of channel arrays. Films with etching times longer than 3 min were also not applied, because of the larger pore size with the relative smaller Debye length and poor effect of the inner wall charge exerted on the ions in the channels. The $I-V$ curves of the two types of films selected for study showed no ionic rectification, signifying symmetry of these nanochannels in structure and surface charge distribution. Moreover, the cross-sectional SEM images of these PET channel arrays verify their columnar structures. All of these details can be seen in Figure S1 (Supporting Information).

DOI: 10.1021/acsami.5b00647
ACS Appl. Mater. Interfaces 2015, 7, 7709−7716

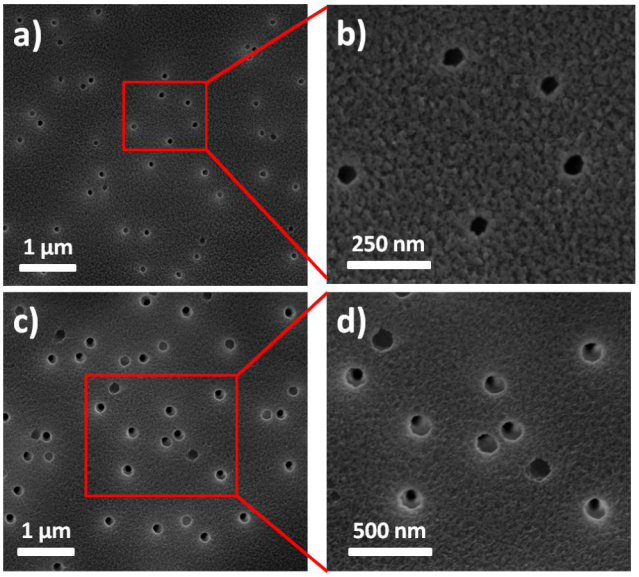

Figure 1. (a,b) SEM images of the PET film etched for 2 min, with pore diameters of 80−90 nm. (c,d) SEM images of the PET film etched for 3 min, with pore diameters of 190−200 nm.

Ion transport in bichannels with the same surface charge but different sizes was studied first. The bichannel device was constructed by stacking two unmodified films with nanochannels with sizes of 80−90 and 190−200 nm together and then carefully located in a custom electrolyte cell. The two half-channels were exposed to the same 0.1 M KCl buffer, and *I*−*V* curves were measured at pH 3 and 11 (Figure 2a). In chemical

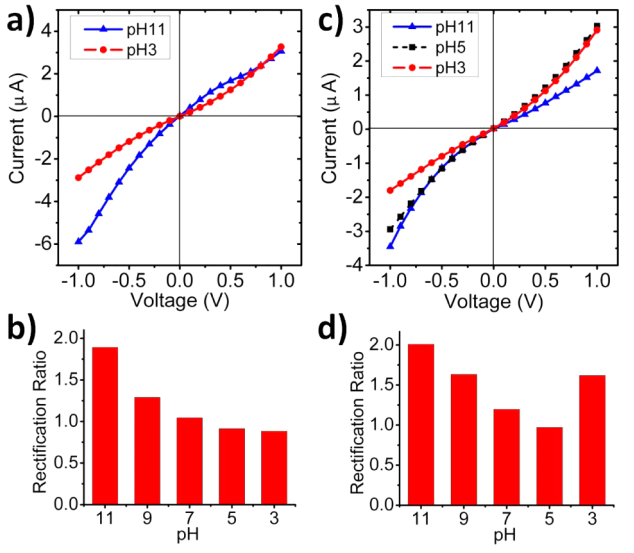

Figure 2. (a,c) *I*−*V* curves of (a) unmodified and (c) histidine-modified bichannels of different sizes at pH 11 (triangles) and pH 3 (circles). (b,d) Changes in the rectification ratio from pH 11 to 3 of the (b) unmodified and (d) histidine-modified bichannels.

etching, many carboxyl groups are produced on the inner surface of the columnar channels. When the pH is above 4, they will be negatively charged. At pH 11, the inner surfaces of the two channels are all negatively charged, and the bichannel shows obvious current rectification. In contrast, at pH 3, the surfaces of the two channels are uncharged, and the bichannel shows no rectification. From pH 11 to 3, the rectification ratio (ratio between the forward current and the reverse current under 1 V) of the entire bichannel decreased from 1.89 to 0.88. (Figure 2b shows the ratio, and the series of *I*−*V* curves from pH 11 to 3 can be seen in Figure S2a, Supporting Information.) These results demonstrate that, by arranging two columnar nanochannel arrays with different pore sizes in a bichannel device, we achieved bichannels with ion current rectification. It is worth noting that the unmodified bichannels with different pore sizes had two pH-dependent states: a nanofluid diode under basic conditions and a normal nanochannel under neutral and acidic conditions, with no current rectification reversal.

After the two channels had been modified with histidine, the pH-dependent regularity of the bichannel in rectification was improved. Histidine, as a basic amino acid, contains a basic amino group, a basic imidazolyl group, and an acidic carboxyl group: The amino group is used for attaching the carboxyl group to the channel surface through a classical EDC-NHSS cross-linking reaction,[49] whereas the same reaction will not occur on the imidazolyl group, and after modification, the remaining imidazolyl and carboxyl groups on the attached molecule will be positively and negatively charged separately in acidic and basic solutions, respectively (Scheme 2). The other

Scheme 2. Change in Surface Charge on the Histidine-Modifeid Bichannel from pH 11 to 3, where the Immobilized Histidine Changes from Negatively Charged to Electroneutral and Then to Positively Charged

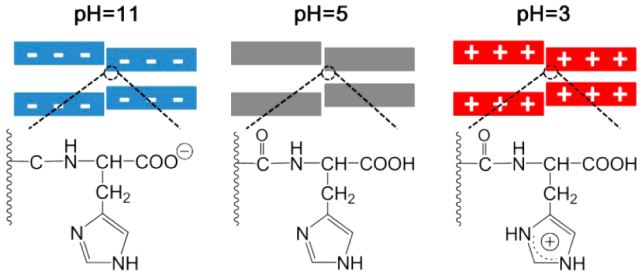

basic amino acids, such as lysine, were not used in this work because they contain two or more amino groups, all of which can react with carboxyl groups on the channel surface during the modification, and cannot supply enough basic groups after that. The success of histidine modification was verified by the X-ray photoelectron spectra of the modified and unmodified films (Figure S3, Supporting Information).

At pH 11, the histidine-modified surfaces of the two half-channels are all negatively charged, showing obvious current rectification in the bichannel device (Figure 2c). At pH 5, both surfaces are uncharged, performing no rectification, whereas at pH 3, the histidine-modified surfaces are positively charged, and the bichannel device manifests rectification opposite to that at pH 11. From pH 11 to 5, the rectification ratio of the histidine-modified bichannel decreases from 2.01 to 0.97. (Figure 2d shows the ratio, and the series of *I*−*V* curves from pH 11 to 3 can be seen in Figure S2b, Supporting Information.) Then, from pH 5 to 3, the rectification ratio increases from 0.97 to 1.62. Thus, compared with the unmodified bichannel , the histidine-modified bichannel with different pore sizes has three pH-dependent states: With a decrease of pH, this device can be converted from a nanofluid diode to a normal nanochannel and then to a reverse nanofluid diode, performing a significant current rectification reversal.

DOI: 10.1021/acsami.5b00647
ACS Appl. Mater. Interfaces 2015, 7, 7709−7716

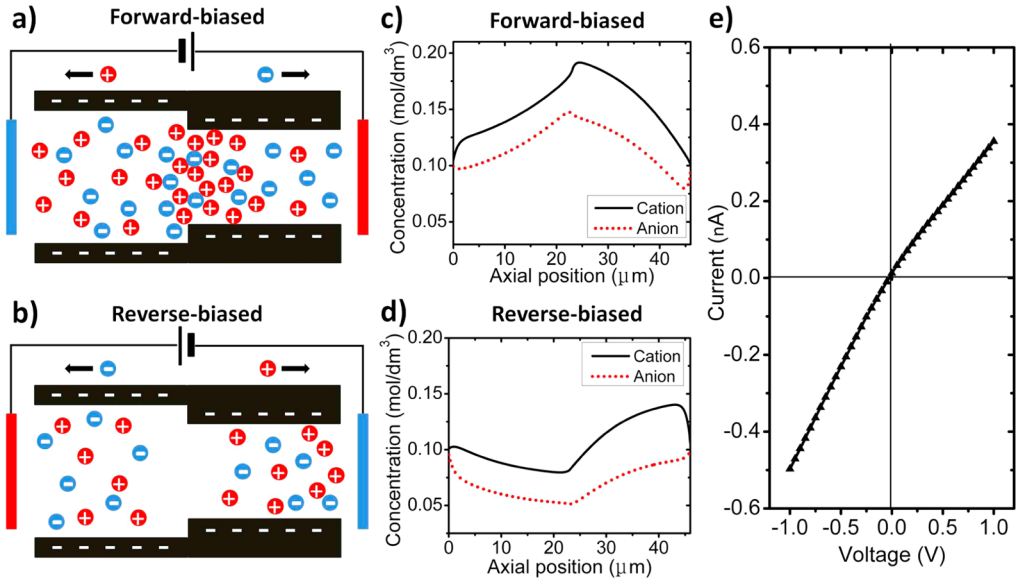

Figure 3. (a) Ion acuumulation and (b) depletion in the forward-biased and reverse-biased bichannels with negative surface charge. (c,d) Ion distributions in the cross section of the negatively charged bichannel calculated by the PNP model under (c) forward and (d) reverse bias. (e) Theoretical *I*−*V* curve of the negatively charged bichannel. A single bichannel was selected for studying in the PNP model, so the calculated currents are on the nanoampere scale.

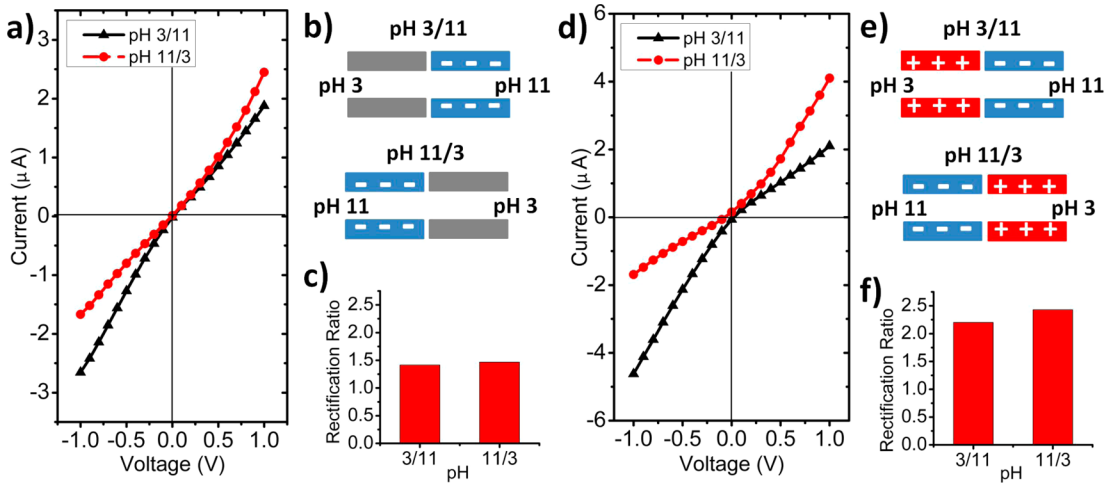

Figure 4. (a,d) *I*−*V* curves of (a) unmodified and (d) histidine-modified bichannels of the same size but asymmetric surface charge at pH 3/11 and 11/3. (b,e) Surface charge polarities of (b) unmodified and (e) modified bichannels. At both pH 3/11 and 11/3, the unmodified bichannel was composed of neutral and negatively charged surfaces, whereas the modified bichannel was composed of positively and negatively charged surfaces. (c,f) Rectification ratios at pH 3/11 and 11/3 for the (c) unmodified and (f) modified bichannels.

The origin of the ion current rectification in the bichannel with different pore sizes is attributed to a cooperative effect on the ions caused by the two columnar nanochannels and the applied electric field.[28,50,51] We take the negatively charged bichannel as an example. For the smaller half-channel in the device, under a forward bias, cations assemble in the junction with the larger one as the electrostatic attraction from the negatively charged surface. In contrast, under a reverse bias, cations are dispelled from the junction. For the larger half-channel in the bichannel, the channel dimensions are far beyond the Debye length, so the surface charge has little effect on mobile ions in the channel. Therefore, when the effects of the two channels are combined, the forward bias causes cation accumulation in the junction of the two channels, accompanied by an anion excess in the same place to maintain electroneutrality (Figure 3a). Similarly, the reverse bias results in the depletion of both ions in the junction (Figure 3b). The ion accumulation and depletion lead to a difference in ionic conductance of the bichannel, generating asymmetric ion transport. Singh and co-workers applied the Poisson/Nernst−Planck (PNP) model to explain ion transport in conical or columnar bipolar nanochannels with smooth junctions.[52−54] Therefore, this model was also applied to explain the current rectification in this work quantitatively, with the calculation details provided in the Supporting Information. The ion distributions in the cross section of the bichannel calculated by the PNP model demonstrate the ion accumulation and depletion under the forward and reverse biases, respectively (Figure 3c,d). The theoretical *I*−*V* curve of the negatively charged bichannel is in agreement with the experimental results (Figure 3e). The positively charged bichannel is just in the

DOI: 10.1021/acsami.5b00647
ACS Appl. Mater. Interfaces 2015, 7, 7709−7716

opposite condition, as also depicted in Figure S4 (Supporting Information).

Next, the ion transport of bichannel devices with the same size but different surface charges was also studied. This type of bichannel device was constructed by stacking two unmodified films with 80−90 nm nanochannels. By exposing the two half-channels of the device to 0.1 M KCl buffers at different pH values, a charged bichannel with different polarities in the two parts was achieved. Here, we chose pH 3 and 11 for a distinct difference in pH between the two half-channels. The current rectification of the unmodified bichannel was a little weak, and the rectification ratio was just 1.41 at pH 3/11 and 1.47 at pH 11/3 (Figure 4a−c). After the two channels had been modified with histidine, the ion current rectification improved significantly, and the rectification ratio of the bichannel increased to 2.20 at pH 3/11 and 2.42 at pH 11/3 (Figure 4d,e). For both the unmodified and histidine-modified bichannels, the reversion of the pH flipped the polarities of the two ends of the bichannel, resulting in an opposite influence on the transfer of ions under the same bias and inducing reverse rectification. Moreover, the results calculated with the PNP model support this explanation (Figures S5 and S6, Supporting Information). Histidine-modified films with 190−200 nm channels were not applied, because this pore size is beyond the Debye length and such channels perform no rectification in the device (Figure S7, Supporting Information).

Other than that, the rectification ratios of histidine-modified bichannels are largely determined by asymmetric pH conditions on the two sides (Figure 5). Such a conclusion is supported by

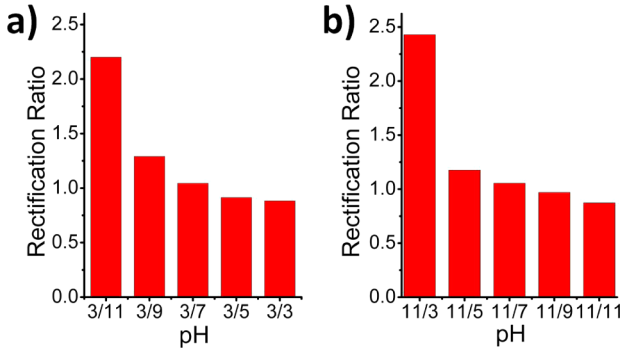

Figure 5. (a) Rectification ratio from pH 3/11 to 3/3; the rectification ratio is I_-/I_+ under 1 V. (b) Rectification ratio from pH 11/3 to 11/11; the rectification ratio is I_+/I_- under 1 V. In both cases, the rectification ratio decreases with the decrease of the pH gap between the two ends of the bichannels.

the following evidence: A histidine-modified bichannel with pH 3 on one side and pH changing from 11 to 3 on the other side exhibits a dramatic decrease of the rectification ratio from 2.20 to 1.20. On the other hand, such a bichannel with pH 11 on one side and pH changing from 3 to 11 exhibits the same decrease, say, 2.42 to 0.87. (The series of $I-V$ curves at different pH values can be seen in Figure S8, Supporting Information.) Experiments such as this illustrate that a large gap between the pH values on the two sides will lead to optimized ion current rectification.

The enhancement and pH-dependent tunability of ion current rectification in the device with histidine modification are due to the difference in the electrostatic interactions applied by the two half-nanochannels to transferring ions, which results from the different degrees of ion excess and deficiency caused by the cooperative effect of the applied electric field and the two half-channels.[55−58] For the unmodified bichannel at pH 3/11, the channel exposed to 0.1 M KCl at pH 3 is uncharged, whereas the channel exposed to 0.1 M KCl at pH 11 is negatively charged (we call it the "semicharged" bichannel). For the histidine-modified bichannel at pH 3/11, the half-channel under acidic conditions is positively charged, whereas the other one under basic conditions is negatively charged (we call it the "bicharged" bichannel). Under a forward bias, in the semicharged bichannel, cations assemble in the junction between the two channels because of the electrostatic attraction from the negatively charged surface (Figure 6a). Similarly, in the bicharged bichannel, cations and anions accumulate in the same place as a result of electrostatic attractions of both the negatively charged surface and the positively charged surface (Figure 6b). Thus, under a forward bias, the degree of cation and anion accumulation in the bicharged bichannel is higher than that in the semicharged bichannel. The ion distributions under a forward bias in bichannels calculated by the PNP model show that the total concentration of both ions in the bicharged bichannel is higher than that in the semicharged bichannel, which means higher ionic conductance (Figure 6c,d). Moreover, the theoretical $I-V$ curves of the two types of bichannels support our explanation (Figure 6e), as the forward currents of the bicharged bichannel are larger than those of the semicharged bichannel. Under a reverse bias, the calculated ion distributions show that ions are dispelled from the junctions in both bichannels and that ion depletion is more obvious in the bicharged bichannel, which means lower ion conductance and smaller reverse currents of the bicharged bichannel (Figures 7 and 6e). Therefore, based on the effect on ion transport under forward and reverse biases, the ion current rectification of the bicharged bichannel is more significant than that in the semicharged bichannel, and histidine modification can improve the current rectification of bichannels with the same size but different pH values. Similarly, for histidine-modified bichannels changing from pH 3/11 to 3/3 (or from pH 11/3 to 11/11), the smaller pH gap between the two ends of the bichannel, which creates less of a difference in the surface charge polarity of the two half-channels, will weaken the electrostatic interaction of the channel surface with the transferring ions and the ionic accumulation/depletion in the channel, thus allowing degraded ion current rectification. Finally, at the same pH, which denotes the same surface charge on the two sides of the channel, a bichannel will perform similarly to a single-column channel with no rectification.

It should be noted that a thin liquid film of 2−3 μm will form by combining two such wetted PET films with nanochannels (Figures S9 and S10, Supporting Information). This liquid film, which serves as a communication vessel to connect the nanochannels on the two PET films, eliminates the blocking to ions caused by the off-axis connection between these nanochannels in the experiments. Because of the thinness of this liquid film, its effect on ion transport can be neglected. As a result, the structure of the bichannels is considered to be matched perfectly in the axial direction and joined tightly for simplification.

CONCLUSIONS

In summary, bichannel devices composed of two PET films with columnar nanochannel arrays varying in size or surface charge all perform obvious ion current rectification. Furthermore, the pH-dependent tunability, along with the rectification

DOI: 10.1021/acsami.5b00647
ACS Appl. Mater. Interfaces 2015, 7, 7709−7716

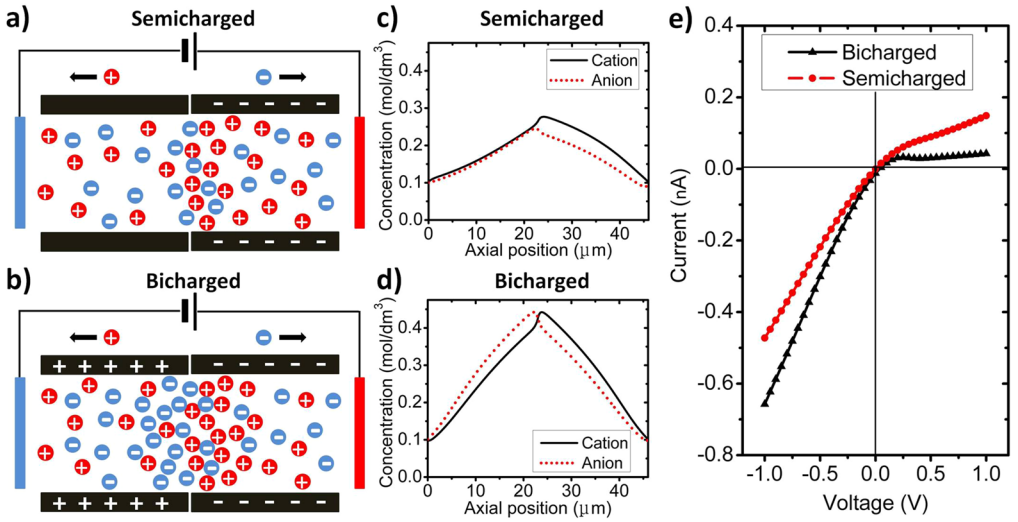

Figure 6. (a,b) Degree of ion accumulation in the forward-biased (a) semicharged and (b) bicharged bichannel. (c,d) Ion distributions of the (c) semicharged and (d) bicharged bichannels under the forward bias calculated by the PNP model. The ion excesses in the junction are significantly different for the two types of bichannels, and ions accumulate more in the bicharged one. (e) Theoretical *I*−*V* curves of the two bichannels.

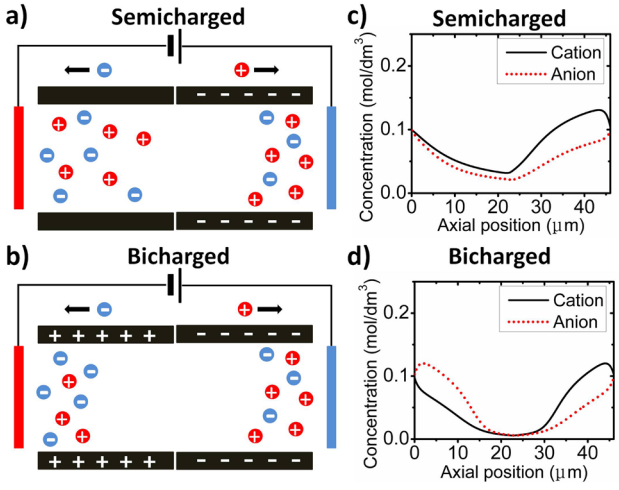

Figure 7. (a,b) Degrees of ion depletion in the reverse-biased (a) semicharged and (b) bicharged bichannels. (c,d) Ion distributions of the (c) semicharged and (d) bicharged bichannels in the reverse bias calculated by the PNP model. The ion deficiency is more serious in the bicharged bichannel.

degree, of the rectification can be improved by histidine modification. The origin of the ion current rectification and its pH-dependent tunability are attributed to the cooperative effect of the two columnar half-channels and the applied bias on mobile ions. As a result of surface groups on the bichannel being charged with different polarities or degrees at different pH values, the bichannel device can be converted from a nanofluid diode to a normal nanochannel or to a reverse diode. Compared with alumina-based multiple-channel devices, the PET bichannel device with columnar nanochannel arrays allows simple and low-cost preparation. In addition, compared with polymer-based counterparts consisting of single conical channels or columnar nanochannels and mesoporous silica, the PET bichannel device allows pH-dependent tunability in ion current rectification. In consideration of these advantages, this type of polymer-based bichannel nanofluidic diode has extensive potential applications in the fields of sensors and material separations.

■ ASSOCIATED CONTENT

Supporting Information

I−*V* curves and cross-sectional SEM image of PET channel arrays, series of *I*−*V* curves with bichannel devices, XPS results, theoretical ion distribution and *I*−*V* curves of bichannels, microscope image of liquid film in bichannel and its influence to ion transport. This material is available free of charge via the Internet at http://pubs.acs.org.

■ AUTHOR INFORMATION

Corresponding Author

*E-mail: zhaijin@buaa.edu.cn.

Notes

The authors declare no competing financial interest.

■ ACKNOWLEDGMENTS

We thank Dafeng Wang (PKU) and Jingtao Wang (BUAA) for beneficial discussions. This work was supported by the National Research Fund for Fundamental Key Projects (2011CB935704, 2012CB720904) and the National Natural Science Foundation (21271016, 91333120).

■ REFERENCES

(1) Gouaux, E.; MacKinnon, R. Principles of Selective Ion Transport in Channels and Pumps. *Science* **2005**, *310*, 1461−1465.
(2) de la Escosura-Muñiz, A.; Merkoçi, A. Nanochannels Preparation and Application in Biosensing. *ACS Nano* **2012**, *6*, 7556−7583.
(3) Nicholson, S. M.; Bruzzone, R. Gap Junctions: Getting the Message Through. *Curr. Biol.* **1997**, *7*, R340−R344.
(4) Kumar, N. M.; Gilula, N. B. The Gap Junction Communication Channel. *Cell* **1996**, *84*, 381−388.
(5) Paul, D. L. New Functions for Gap Junctions. *Curr. Opin. Cell Biol.* **1995**, *7*, 665−672.
(6) Wen, L.; Hou, X.; Tian, Y.; Nie, F.-Q.; Song, Y.; Zhai, J.; Jiang, L. Bioinspired Smart Gating of Nanochannels Toward Photoelectric-Conversion Systems. *Adv. Mater.* **2010**, *22*, 1021−1024.
(7) Wen, L.; Jiang, L. Construction of Biomimetic Smart Nanochannels for Confined Water. *Natl. Sci. Rev.* **2014**, *1*, 144−156.
(8) Kong, Y.; Fan, X.; Zhang, M.; Hou, X.; Liu, Z.; Zhai, J.; Jiang, L. Nanofluidic Diode Based on Branched Alumina Nanochannels with Tunable Ionic Rectification. *ACS Appl. Mater. Interfaces* **2013**, *5*, 7931−7936.

DOI: 10.1021/acsami.5b00647
ACS Appl. Mater. Interfaces 2015, 7, 7709−7716

(9) Chen, W.; Wu, Z.-Q.; Xia, X.-H.; Xu, J.-J.; Chen, H.-Y. Anomalous Diffusion of Electrically Neutral Molecules in Charged Nanochannels. *Angew. Chem., Int. Ed.* **2010**, *49*, 7943−7947.
(10) Liu, N.; Chen, Z.; Dunphy, D. R.; Jiang, Y.-B.; Assink, R. A.; Brinker, C. J. Photoresponsive Nanocomposite Formed by Self-Assembly of an Azobenzene-Modified Silane. *Angew. Chem., Int. Ed.* **2003**, *42*, 1731−1734.
(11) Cheng, L.-J.; Guo, L. J. Rectified Ion Transport through Concentration Gradient in Homogeneous Silica Nanochannels. *Nano Lett.* **2007**, *7*, 3165−3171.
(12) Pavan Kumar, B. V. V. S.; Venkata Rao, K.; Sampath, S.; George, S. J.; Eswaramoorthy, M. Supramolecular Gating of Ion Transport in Nanochannels. *Angew. Chem., Int. Ed.* **2014**, *53*, 13073−13077.
(13) Fernandez, I.; Sanchez, A.; Diez, P.; Martinez-Ruiz, P.; Di Pierro, P.; Porta, R.; Villalonga, R.; Pingarron, J. M. Nanochannel-Based Electrochemical Assay for Transglutaminase Activity. *Chem. Commun.* **2014**, *50*, 13356−13358.
(14) Hu, Z.; Zhang, Q.; Gao, J.; Liu, Z.; Zhai, J.; Jiang, L. Photocatalysis-Triggered Ion Rectification in Artificial Nanochannels Based on Chemically Modified Asymmetric TiO_2 Nanotubes. *Langmuir* **2013**, *29*, 4806−4812.
(15) Zhang, Q.; Liu, Z.; Hou, X.; Fan, X.; Zhai, J.; Jiang, L. Light-Regulated Ion Transport through Artificial Ion Channels Based on TiO_2 Nanotubular Arrays. *Chem. Commun.* **2012**, *48*, 5901.
(16) Lanyon, Y. H.; De Marzi, G.; Watson, Y. E.; Quinn, A. J.; Gleeson, J. P.; Redmond, G.; Arrigan, D. W. M. Fabrication of Nanopore Array Electrodes by Focused Ion Beam Milling. *Anal. Chem.* **2007**, *79*, 3048−3055.
(17) Karnik, R.; Duan, C.; Castelino, K.; Daiguji, H.; Majumdar, A. Rectification of Ionic Current in a Nanofluidic Diode. *Nano Lett.* **2007**, *7*, 547−551.
(18) Keyser, U. F.; Koeleman, B. N.; van Dorp, S.; Krapf, D.; Smeets, R. M. M.; Lemay, S. G.; Dekker, N. H.; Dekker, C. Direct Force Measurements on DNA in a Solid-State Nanopore. *Nat. Phys.* **2006**, *2*, 473−477.
(19) Zhang, L.-X.; Cai, S.-L.; Zheng, Y.-B.; Cao, X.-H.; Li, Y.-Q. Smart Homopolymer Modification to Single Glass Conical Nanopore Channels: Dual-Stimuli-Actuated Highly Efficient Ion Gating. *Adv. Funct. Mater.* **2011**, *21*, 2103−2107.
(20) Liu, J.; Kvetny, M.; Feng, J.; Wang, D.; Wu, B.; Brown, W.; Wang, G. Surface Charge Density Determination of Single Conical Nanopores Based on Normalized Ion Current Rectification. *Langmuir* **2011**, *28*, 1588−1595.
(21) Sa, N.; Fu, Y.; Baker, L. A. Reversible Cobalt Ion Binding to Imidazole-Modified Nanopipettes. *Anal. Chem.* **2010**, *82*, 9963−9966.
(22) Lan, W.-J.; Holden, D. A.; White, H. S. Pressure-Dependent Ion Current Rectification in Conical-Shaped Glass Nanopores. *J. Am. Chem. Soc.* **2011**, *133*, 13300−13303.
(23) White, H. S.; Bund, A. Ion Current Rectification at Nanopores in Glass Membranes. *Langmuir* **2008**, *24*, 2212−2218.
(24) Zhang, H.; Hou, X.; Zeng, L.; Yang, F.; Li, L.; Yan, D.; Tian, Y.; Jiang, L. Bioinspired Artificial Single Ion Pump. *J. Am. Chem. Soc.* **2013**, *135*, 16102−16110.
(25) Wen, L.; Tian, Y.; Guo, Y.; Ma, J.; Liu, W.; Jiang, L. Conversion of Light to Electricity by Photoinduced Reversible pH Changes and Biomimetic Nanofluidic Channels. *Adv. Funct. Mater.* **2013**, *23*, 2887−2893.
(26) Tahir, M. N.; Ali, M.; Andre, R.; Muller, W. E. G.; Schroder, H.-C.; Tremel, W.; Ensinger, W. Silicatein Conjugation inside Nano-confined Geometries through Immobilized NTA-Ni(II) Chelates. *Chem. Commun.* **2013**, *49*, 2210−2212.
(27) Siwy, Z.; Apel, P.; Dobrev, D.; Neumann, R.; Spohr, R.; Trautmann, C.; Voss, K. Ion Transport through Asymmetric Nanopores Prepared by Ion Track Etching. *Nucl. Instrum. Methods Phys. Res. B* **2003**, *208*, 143−148.
(28) Li, C.-Y.; Ma, F.-X.; Wu, Z.-Q.; Gao, H.-L.; Shao, W.-T.; Wang, K.; Xia, X.-H. Solution-pH-Modulated Rectification of Ionic Current in Highly Ordered Nanochannel Arrays Patterned with Chemical Functional Groups at Designed Positions. *Adv. Funct. Mater.* **2013**, *23*, 3836−3844.
(29) Han, J.-H.; Kim, K. B.; Kim, H. C.; Chung, T. D. Ionic Circuits Based on Polyelectrolyte Diodes on a Microchip. *Angew. Chem., Int. Ed.* **2009**, *48*, 3830−3833.
(30) Woermann, D. Electrochemical Transport Properties of a Cone-Shaped Nanopore: Revisited. *Phys. Chem. Chem. Phys.* **2004**, *6*, 3130−3132.
(31) Schmuhl, R.; Sekulic, J.; Roy Chowdhury, S.; van Rijn, C. J. M.; Keizer, K.; van den Berg, A.; ten Elshof, J. E.; Blank, D. H. A. Si-Compatible Ion-Selective Oxide Interconnects with High Tunability. *Adv. Mater.* **2004**, *16*, 900−904.
(32) Zhang, Q.; Hu, Z.; Liu, Z.; Zhai, J.; Jiang, L. Light-Gating Titania/Alumina Heterogeneous Nanochannels with Regulatable Ion Rectification Characteristic. *Adv. Funct. Mater.* **2014**, *24*, 424−431.
(33) Gao, J.; Guo, W.; Feng, D.; Wang, H.; Zhao, D.; Jiang, L. High-Performance Ionic Diode Membrane for Salinity Gradient Power Generation. *J. Am. Chem. Soc.* **2014**, *136*, 12265−12272.
(34) Cheng, L.-J.; Guo, L. J. Ionic Current Rectification, Breakdown, and Switching in Heterogeneous Oxide Nanofluidic Devices. *ACS Nano* **2009**, *3*, 575−584.
(35) Yamaguchi, A.; Uejo, F.; Yoda, T.; Uchida, T.; Tanamura, Y.; Yamashita, T.; Teramae, N. Self-Assembly of a Silica−Surfactant Nanocomposite in a Porous Alumina Membrane. *Nat. Mater.* **2004**, *3*, 337−341.
(36) Zhang, W.; Meng, Z.; Zhai, J.; Heng, L. Ion Current Behaviors of Mesoporous Zeolite-Polymer Composite Nanochannels Prepared by Water-Assisted Self-Assembly. *Chem. Commun.* **2014**, *50*, 3552−3555.
(37) Zeng, L.; Yang, Z.; Zhang, H.; Hou, X.; Tian, Y.; Yang, F.; Zhou, J.; Li, L.; Jiang, L. Tunable Ionic Transport Control inside a Bio-Inspired Constructive Bi-Channel Nanofluidic Device. *Small* **2014**, *10*, 793−801.
(38) Wen, L.; Liu, Q.; Ma, J.; Tian, Y.; Li, C.; Bo, Z.; Jiang, L. Malachite Green Derivative−Functionalized Single Nanochannel: Light-and-pH Dual-Driven Ionic Gating. *Adv. Mater.* **2012**, *24*, 6193−6198.
(39) Nasir, S.; Ali, M.; Ensinger, W. Thermally Controlled Permeation of Ionic Molecules through Synthetic Nanopores Functionalized with Amine-Terminated Polymer Brushes. *Nanotechnology* **2012**, *23*, 225502.
(40) Yameen, B.; Ali, M.; Neumann, R.; Ensinger, W.; Knoll, W.; Azzaroni, O. Synthetic Proton-Gated Ion Channels via Single Solid-State Nanochannels Modified with Responsive Polymer Brushes. *Nano Lett.* **2009**, *9*, 2788−2793.
(41) Vlassiouk, I.; Kozel, T. R.; Siwy, Z. S. Biosensing with Nanofluidic Diodes. *J. Am. Chem. Soc.* **2009**, *131*, 8211−8220.
(42) Orelovich, O. L.; Sartowska, B. A.; Presz, A.; Apel, P. Y. Analysis of Channel Shapes in Track Membranes by Scanning Electron Microscopy. *J. Microsc.* **2010**, *237*, 404−406.
(43) Chtanko, N.; Toimil Molares, M. E.; Cornelius, T.; Dobrev, D.; Neumann, R. Etched Single-Ion-Track Templates for Single Nanowire Synthesis. *J. Phys. Chem. B* **2004**, *108*, 9950−9954.
(44) Meng, Z.; Jiang, C.; Li, X.; Zhai, J. Calcein-Modified Multinanochannels on PET Films for Calcium-Responsive Nanogating. *ACS Appl. Mater. Interfaces* **2014**, *6*, 3794−3798.
(45) Meng, Z.; Bao, H.; Wang, J.; Jiang, C.; Zhang, M.; Zhai, J.; Jiang, L. Artificial Ion Channels Regulating Light-Induced Ionic Currents in Photoelectrical Conversion Systems. *Adv. Mater.* **2014**, *26*, 2329−2334.
(46) Hou, X.; Dong, H.; Zhu, D.; Jiang, L. Fabrication of Stable Single Nanochannels with Controllable Ionic Rectification. *Small* **2010**, *6*, 361−365.
(47) Kalman, E. B.; Vlassiouk, I.; Siwy, Z. S. Nanofluidic Bipolar Transistors. *Adv. Mater.* **2008**, *20*, 293−297.
(48) Siwy, Z. S. Ion-Current Rectification in Nanopores and Nanotubes with Broken Symmetry. *Adv. Funct. Mater.* **2006**, *16*, 735−746.

DOI: 10.1021/acsami.5b00647
ACS Appl. Mater. Interfaces 2015, 7, 7709−7716

(49) Hou, X.; Zhang, H.; Jiang, L. Building Bio-Inspired Artificial Functional Nanochannels: From Symmetric to Asymmetric Modification. *Angew. Chem., Int. Ed.* **2012**, *51*, 5296−5307.
(50) Hsu, W.-L.; Inglis, D. W.; Startsev, M. A.; Goldys, E. M.; Davidson, M. R.; Harvie, D. J. E. Isoelectric Focusing in a Silica Nanofluidic Channel: Effects of Electromigration and Electroosmosis. *Anal. Chem.* **2014**, *86*, 8711−8718.
(51) Pu, Q.; Yun, J.; Temkin, H.; Liu, S. Ion-Enrichment and Ion-Depletion Effect of Nanochannel Structures. *Nano Lett.* **2004**, *4*, 1099−1103.
(52) Singh, K. P.; Kumar, M. Effect of Nanochannel Diameter and Debye Length on Ion Current Rectification in a Fluidic Bipolar Diode. *J. Phys. Chem. C* **2011**, *115*, 22917−22924.
(53) Singh, K. P.; Kumari, K.; Kumar, M. Ion Current Rectification in a Fluidic Bipolar Nanochannel with Smooth Junction. *Appl. Phys. Lett.* **2011**, *99*, 113103.
(54) Singh, K. P.; Kumar, M. Effect of Surface Charge Density and Electro-Osmotic Flow on Ionic Current in a Bipolar Nanopore Fluidic Diode. *J. Appl. Phys.* **2011**, *110*, 084322.
(55) Daiguji, H. Ion Transport in Nanofluidic Channels. *Chem. Soc. Rev.* **2010**, *39*, 901−911.
(56) Cheng, L.-J.; Guo, L. J. Nanofluidic Diodes. *Chem. Soc. Rev.* **2010**, *39*, 923−938.
(57) He, Y.; Gillespie, D.; Boda, D.; Vlassiouk, I.; Eisenberg, R. S.; Siwy, Z. S. Tuning Transport Properties of Nanofluidic Devices with Local Charge Inversion. *J. Am. Chem. Soc.* **2009**, *131*, 5194−5202.
(58) Daiguji, H.; Oka, Y.; Shirono, K. Nanofluidic Diode and Bipolar Transistor. *Nano Lett.* **2005**, *5*, 2274−2280.

DOI: 10.1021/acsami.5b00647
ACS Appl. Mater. Interfaces 2015, 7, 7709−7716